Measurements of Pion and Muon Nuclear Capture at Rest on Argon in the LArIAT Experiment

M. A. Hernandez-Morquecho,[1] R. Acciarri,[2] J. Asaadi,[3] M. Backfish,[2,*] W. Badgett,[2] V. Basque,[2] F. d. M. Blaszczyk,[2] W. Foreman,[1,†] R. A. Gomes,[4] E. Gramellini,[5] J. Ho,[6,‡] E. Kearns,[7] E. Kemp,[8] T. Kobilarcik,[2] M. King,[6] B. R. Littlejohn,[1] X. Luo,[9] A. Marchionni,[2] C. A. Moura,[10] J. L. Raaf,[2] D. W. Schmitz,[6] M. Soderberg,[11] J. M. St. John,[2] A. M. Szelc,[12] and T. Yang[2]

(LArIAT Collaboration)[§]

[1]*Illinois Institute of Technology, Chicago, Illinois 60616, USA*
[2]*Fermi National Accelerator Laboratory, Batavia, Illinois 60510, USA*
[3]*University of Texas at Arlington, Arlington, Texas 76019, USA*
[4]*Universidade Federal de Goiás, Goiás, CEP 74690-900, Brazil*
[5]*Yale University, New Haven, Connecticut 06520, USA*
[6]*University of Chicago, Chicago, Illinois 60637, USA*
[7]*Boston University, Boston, Massachusetts 02215, USA*
[8]*Universidade Estadual de Campinas, Campinas, Sao Paulo 13083-859, Brazil*
[9]*University of California, Santa Barbara, California 93106, USA*
[10]*Universidade Federal do ABC, Santo André, Sao Paulo 09210-580, Brazil*
[11]*Syracuse University, Syracuse, New York 13244, USA*
[12]*University of Edinburgh, Edinburgh EH8 9YL, United Kingdom*

(Received 20 August 2024; accepted 12 February 2025; published 1 April 2025)

We report the measurement of the final-state products of negative pion and muon nuclear capture at rest on argon by the LArIAT experiment at the Fermilab Test Beam Facility. We measure a population of isolated MeV-scale energy depositions, or blips, in 296 LArIAT events containing tracks from stopping low-momentum pions and muons. The average numbers of visible blips are measured to be 0.74 ± 0.19 and 1.86 ± 0.17 near muon and pion track endpoints, respectively. The 3.6σ statistically significant difference in blip content between muons and pions provides the first demonstration of a new method of pion-muon discrimination in neutrino liquid argon time projection chamber experiments. LArIAT Monte Carlo simulations predict substantially higher average blip counts for negative muon (1.22 ± 0.08) and pion (2.34 ± 0.09) nuclear captures. We attribute this difference to GEANT4's inaccurate simulation of the nuclear capture process.

DOI: 10.1103/PhysRevLett.134.131801

Liquid argon time projection chambers (LArTPCs) present a unique combination of large detector mass, excellent spatial resolution, and low detection thresholds that make them attractive for novel particle and nuclear physics measurements. By testing single-phase LArTPC capabilities at the MeV and sub-MeV scale—the lowest end of their dynamic range in energy—neutrino experiments have provided first measurements of final-state neutrons from neutrino-argon nuclear interactions [1], performed sensitive searches for millicharged particles [2], and measured radioactive contaminants present in large neutrino LArTPC detectors [3,4]. Other recent literature has more broadly explored the range of potential applications of low-energy thresholds and MeV-scale energy reconstruction in neutrino LArTPC physics [5–9].

A subset of these studies has considered the use of low-energy signatures in performing charge-sign and particle species identification for pions (π) and muons (μ) in LArTPCs [5,7]. Muon charge-sign selection offers obvious

[*]Present address: University of California, Davis, California 95616, USA.
[†]Present address: Los Alamos National Laboratory, Los Alamos, New Mexico 87545, USA.
[‡]Present address: Harvard University, Cambridge, Massachusetts 02138, USA.
[§]Contact author: lariat_authors@fnal.gov

advantages for beam neutrino oscillation physics by reducing wrong-sign contamination during antineutrino-mode run configurations [10–12]. Meanwhile, separation of particle species is an important consideration for π-focused neutrino-nucleus interaction cross-section measurements [13–20] and new physics searches involving π/μ final states [21–27]. Prior measurements along these lines have leveraged a variety of π/μ and/or charge-sign discrimination techniques, including detector magnetization [28,29], charged particle track length comparisons, Michel electron identification [19,20], and kinked track identification [13]. While the mm-scale position resolution and scintillation-based or ionization-based calorimetric attributes of LArTPCs appear amenable to many of these techniques, no existing studies have directly demonstrated LArTPC capabilities in this regard.

In this Letter, we investigate an entirely new particle discrimination technique that uniquely leverages an LArTPC's low-energy reconstruction capabilities. As they range out in large detectors, π^- and μ^- will preferentially experience nuclear capture: $\pi^- + {}^{40}\mathrm{Ar} \rightarrow {}^{40}\mathrm{Cl}*$ occurs nearly 100% of the time for stopped π^- in argon, while $\mu^- + {}^{40}\mathrm{Ar} \rightarrow {}^{40}\mathrm{Cl} * + \nu_\mu$ occurs for 70%–75% of stopped μ^- [5,30]. Nuclear captures generate MeV-scale deexcitation products (γ rays and neutrons), which interact in the surrounding liquid argon to produce displaced energy depositions reconstructed as "blips" of charge spanning only a few readout wires. This distinct final-state topology differs from that of free π^+/μ^+ decay. Likewise, since π deposit more rest-mass energy in capturing nuclei than μ, more blip features should accompany their capture. Prior LArTPC simulation studies have provided a first look at the quantitative benefits of this technique while commenting on its complementariness with respect to other potential discrimination techniques in LArTPCs [5].

Measurements of the products of π/μ nuclear capture at rest on argon are scarce: only one measurement for μ reports the prevalence of various unstable final-state nuclei [31], and no measurements exist for π. Existing predictions of final states in particle transport simulations such as GEANT4 [32] and FLUKA [33] are based on nuclear models benchmarked to measurements of various medium-energy nuclear processes on other target nuclei. Beyond demonstrating the viability of capture-based π/μ discrimination or testing the accuracy of particle transport simulations, a measurement of the products of muon nuclear capture at rest provides insight into the related weak process of low-energy muon neutrino charged-current absorption [34]. An argon-based π/μ nuclear capture measurement thus serves as a reference point for low-energy neutrino interaction generators [35] used for performing neutrino astrophysics in large LArTPCs [6,36,37]. It provides a similar reference point for aspects of high-energy neutrino interaction models [38–41].

In this Letter, we present measurements of the final-state products of π^- and μ^- nuclear capture at rest (πCAR and μCAR) on argon using the Liquid Argon In A Testbeam (LArIAT) experiment at Fermilab. Final-state γ ray and neutron content is reported in terms of the properties of reconstructed low-energy mm-scale blips generated by these particles in LArTPC events. Blip counts are found to be higher in events containing πCAR and μCAR than in background events containing only throughgoing beam particles. A higher count in πCAR than in μCAR events provides the first demonstration of blip-based particle discrimination. LArIAT Monte Carlo (MC) simulations predict higher blip counts near nuclear captures than observed in data, suggesting improper modeling of nuclear deexcitation processes in the GEANT4 particle transport code.

The LArIAT experiment was operated from 2015 to 2017 in a tertiary particle beamline in the MC7 hall at Fermilab's Test Beam Facility. Detailed descriptions of the beam and LArTPC are given in Ref. [42]. Tertiary beam particles ($e^\pm$, $\mu^\pm$, $\pi^\pm$, $p^\pm$, $K^\pm$, etc.) were produced for LArIAT by colliding a 64 GeV/c peak momentum π^+-dominated secondary beam into a copper target. Boosted, charged products were collimated and then steered via two electromagnets through beam instrumentation that included four position-measuring multiwire proportional chambers (MWPCs) and two time-of-flight (TOF) scintillator paddles. Tuning of beam momentum and charge sign was performed by adjusting the electromagnet current. The momentum of individual particles, ranging between 275 and 1400 MeV/c, was determined by measuring the bending radius using two MWPCs upstream and downstream from the electromagnet. Particle momenta upon entering the LArIAT LArTPC are lower than beam-reported values due to energy loss in materials between the downstream wire chamber and the active time projection chamber (TPC) volume. Combined momentum and TOF measurements enabled clean separation of beam $\pi/\mu/e$ from heavier particle species. While particles primarily traverse the beamline individually, pileup muons and neutrons produced in the primary or secondary targets are also present in MC7 and are not monitored by LArIAT beamline instrumentation.

The LArIAT cryostat is located approximately 10 cm past the downstream-most TOF detector. Filled with 0.76 t of liquid argon, it contains the LArIAT LArTPC, a $47 \times 40 \times 90$ cm^3, 0.24 t active chamber equipped with a uniform 490 V/cm electric field along the drift direction (x in LArIAT's coordinate system). The TPC electric field is perpendicular to the beam particle direction (z). Ionization generated by beam particles is drifted a maximum x distance of 47 cm toward two planes of conducting sense wires. For Run II, each plane is made of 240 wires spaced 4 mm apart and oriented $\pm 60°$ with respect to the vertical (y) direction. The drifting charge produces signals

on the two instrumented wire planes by passing by the first (induction plane) and collecting on the second (collection plane). These signals are amplified, shaped, and digitized to generate 3072-sample waveforms with a sampling period of 0.128 μs per time tick, for a total readout time of 393 μs—sufficient to record all ionization activity occurring within the full 320 μs drift period as well as some ionization occurring before and after the beam-triggered event. Triggering of TPC readout is initiated by coincident signals from the Fermilab Test Beam Facility primary beamline, all MWPCs and TOF beamline instruments, and the LArTPC's scintillation light collection system [30]. Roughly 20–50 triggers were recorded over each 4.2 s beam spill delivered to LArIAT once every 60.5 s, with 10 triggers free of beam activity (referred to as pedestal triggers) recorded before each spill.

For this Letter, we use data from LArIAT's Run II-A and II-B campaigns, collected between February and July 2016. Since the study concerns low-momentum beam μ^- and π^- capable of stopping in the TPC and undergoing nuclear capture, data from LArIAT's low-energy negative beam tuning were considered. Since LArIAT did not employ a liquid argon recirculation and purification system [42], a subset of runs exhibited poor liquid argon purity. To account for this, runs with electron lifetimes lower than 320 μs—the approximate cathode-to-anode drift time—were excluded from further analysis. These requirements leave a total of 62 452 beam and 201 593 pedestal triggers for analysis.

Procedures for reconstructing high-level physics objects from LArIAT wire analog-to-digital (ADC) waveforms are typical of a single-phase LArTPC [43], and are described in detail in Ref. [44]. After deconvolving the collection and induction plane ADC waveforms using the known response function of LArIAT's electronics, output unipolar signals are scanned for threshold-crossing features, or hits, which are assigned time, width, and amplitude attributes using a Gaussian fit. Hit amplitudes can be converted into reconstructed collected charges using electron lifetime and per-channel gain calibration constants derived using TPC-traversing cosmic and beam muons. Linearly arranged wire- and time-adjacent hit groups on the two wire planes are matched and clustered to form 3D reconstructed tracks [45].

All hits that were not directly included in reconstructed 3D tracks > 5 cm in length are used as input to reconstruct isolated low-energy depositions, or blips. Blip reconstruction in LArIAT proceeds similarly to that reported by previous experiments [1,4]. Time- and wire-adjacent hits are grouped into 2D clusters, which are matched between planes to form a 3D blip using the coincident time ticks and recorded charges. Topologies for reconstructed blips vary from compact mm-scale objects with a single hit on each plane to comparatively extended objects with cm-scale bloblike or tracklike attributes. A blip's y and z coordinates are determined by the location of crossing wires associated with the blip's highest-amplitude hit from each plane, while the blip's x coordinate is calculated based on its drift time and the measured electron drift velocity. To reconstruct a blip's electron-equivalent deposited energy, E_{blip}, a linear charge-to-energy conversion is used based on the integrated charge on the collection plane [4]. Resulting blip reconstruction efficiency at the dataset's mean electron lifetime of 450 μs, determined using MC simulations of single uniformly distributed electrons in the active TPC, exceeds 95% above 0.3 MeV, while dropping to 50% at 0.22 MeV and approaching 0% at 0.13 MeV. Blip efficiencies in E_{blip} and in x vary from run to run due to large lifetime variations over the data-taking period, an effect that is accounted for in LArIAT beam MC simulations and systematic uncertainty estimates.

A series of selection cuts on beam wire chamber and TPC track information were used to isolate a pure sample of events with a nuclear capture of a stopped π^- or μ^- within the active TPC. To illustrate applied cuts, a selected data event display is shown in Fig. 1. First, the entry point of an event's beam particle into the TPC, as projected by the MWPCs, was required to match the upstream starting point of a reconstructed TPC track within a 2 cm radius (referred to as a MWPC-TPC match). Next, to study only the subset of these signal beam particles capable of ranging out inside the TPC, only beam particles with momentum < 415 MeV/c were kept. In selected events, the signal TPC track must be > 35 cm long, and while it must start < 5 cm from the upstream TPC face, it cannot be throughgoing, i.e., also having an endpoint < 2 cm from the TPC's back face. To keep stopping signal tracks with an observable Bragg peak, the median $\mathrm{d}E/\mathrm{d}x$ of all hits within the last 6 cm of this track was required to be > 3 MeV/cm.

Coincident activity from pileup beam muons was reduced by requiring four or fewer total tracks, and all nonsignal throughgoing tracks were required to be > 8 cm from the signal track. To categorize remaining events into πCAR and μCAR samples, we compared their

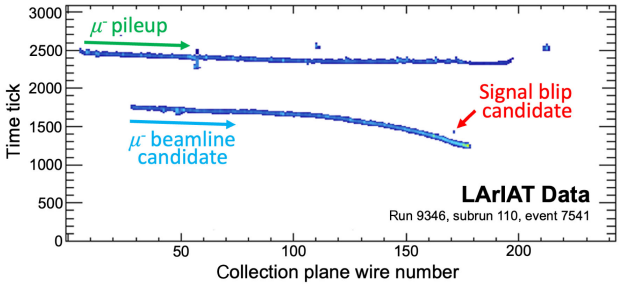

FIG. 1. A raw LArIAT data event display showing a candidate muon nuclear capture at rest. MeV-scale blip activity is visible near the signal track's endpoint. Background tracks and blips further from this endpoint, caused primarily by pileup beam muons and neutrons, are also visible in the event. A rainbow color scale is used to indicate ADC signal amplitude per readout time tick.

reconstructed beam momentum, p (in MeV/c), and TPC signal track range, L (in cm), with boundaries optimized based on LArIAT beam particle MC simulations described in the subsequent material. As illustrated in the accompanying Supplemental Material (SM) [46], these categories were determined by evaluating L in relation to the functional form predicting track length based on beam particle momentum, $Ap - B$. Events satisfying $L > 0.43p - 79.5$ were categorized as μCAR candidates, while tracks with length ranging between this boundary and $L > 0.41p - 86.5$ were categorized as πCAR candidates. These requirements result in the selection of 87 and 209 μCAR and πCAR signal events, respectively.

LArIAT beamline simulation tools, previously described in Ref. [44], were used to generate a MC beam dataset roughly 5 times larger than the analyzed dataset. Generation of tertiary beam particles and their propagation downstream to the final wire chamber were simulated using G4BEAMLINE [47]. Particle transport and detector response were simulated using LARSOFT [48] v08_38_01, which employs GEANT4 v4_10_3_p03e [32]. Beam pileup muons were also simulated using LARSOFT, with counts and trajectories dictated by analysis of real beam data. MC-predicted efficiencies for selecting μCAR and πCAR events with the analysis cuts above, shown in Table I, are 52%, while predicted signal purity is 79% and 76%, respectively. A large majority of backgrounds in the μCAR sample are muon decays at rest (μDAR), while backgrounds for the πCAR sample are split primarily between μCAR-terminating tracks, inelastically scattering pions, and pions absorbed in flight. A comparison of data and MC signal track variables for selected πCAR and μCAR events are also presented in the accompanying SM [46].

With a purified selected sample of nuclear capture events in hand, we turn to studying the reconstructed blips produced by the captures' final-state products. To remove activity from track δ rays and bremsstrahlung radiation, we exclude blips within 2 cm of any reconstructed track, as well as all blips with $E_{\text{blip}} > 3$ MeV. To avoid complexities in reconstructing activity at a particle's stopping point, we also cut blips appearing within 3 cm of the signal track's endpoint. As summarized in Table II, this selection yields an average of 5.23 and 6.42 blips per event in the selected μCAR and πCAR datasets.

Blips in selected events are generated by a combination of true stopped beam particle nuclear captures (signal), beam particles undergoing other nuclear interactions, pileup beam muons, incorrect matches between unrelated features on induction and collection planes, ambient noise and radiogenic signatures, and pileup neutrons. Blip contributions from the first four categories can be estimated using the LArIAT beam MC simulations. To quantify expected ambient noise and radiogenic blip populations, identical blip selection criteria were applied to the off-beam pedestal dataset, yielding a subdominant 0.36 blips per event. Since pileup beam neutrons were not simulated, their contributions were estimated using a set of 513 events containing throughgoing signal tracks with measured beam momentum between 440 and 500 MeV/c. By subtracting blip attributes of the throughgoing dataset from signal μCAR and πCAR datasets, we remove all contributions from sources unrelated to the beam particle's terminating process. The average blip count per event in the throughgoing event dataset is also given in Table II. A check of blip counts at $z < 35$ cm, a TPC region hosting almost no signal track endpoints, reveals identical results between throughgoing and combined signal datasets—averaging roughly 1.57 blips per event within ±5.5% statistical uncertainty—indicating that the background-subtraction method works as expected. A similar $z < 35$ cm requirement applied to the LArIAT MC dataset yields a blip count of only 0.21 per event. This demonstrates that most background blips in this analysis are produced by the unsimulated population of pileup beam neutrons, which is correctly accounted for with the data-driven method described above.

Figure 2 shows the distance from each blip to its corresponding track's endpoint for signal and throughgoing events. To maintain a similar blip selection efficiency in throughgoing events, which do not contain a track endpoint

TABLE I. Summary of signal selection cuts and associated data reduction and signal purity expectations. Event counts reduce moving down the table as cuts are successively added.

		MC		
Cut		All	μCAR	πCAR
MWPC-TPC match		148 834	3231	5769
Beam momentum		35 654	3231	5562
Signal track selection		35 031	3195	5480
Bragg peak		10 283	1912	3619
Total track number		9457	1793	3404
Particle range	(μ)	2132	1686	3
Requirement	(π)	3931	61	2984
Selected	(μ)	0.014	0.52	< 0.01
Fraction	(π)	0.026	0.02	0.52
Purity	(μ)	⋯	0.79	⋯
	(π)	⋯	⋯	0.76

TABLE II. Blip counts per event for background data and for signal data and MC. Bolded parenthesized values indicate counts for the volume < 25 cm from the signal track endpoint.

		Signal		
Dataset	Throughgoing background	Raw	Subtracted	MC
μCAR	4.30	5.23	0.93	1.34
		(**1.69**)	(**0.74**)	(**1.22**)
πCAR	(**0.95**)	6.42	2.12	2.93
		(**2.81**)	(**1.86**)	(**2.34**)

in the TPC's bulk, this variable is defined for thorough-going events by taking the distance from each blip in the event to a signal track endpoint vertex of a randomly chosen signal μCAR or πCAR event, similarly to Ref. [1]. As expected, blip counts at long distances are comparable between datasets. However, at short distances counts deviate well beyond the dominant statistical errors of the two datasets. This difference is highlighted in Table II, which quotes average blip counts for the region within 25 cm of a signal track endpoint: after background subtraction, an average blip count of 0.74 ± 0.19 and 1.86 ± 0.17 per event is observed near muon and pion capture points, respectively. A χ^2 comparison between throughgoing and μCAR (πCAR) samples in Fig. 2 yields 47.7 (251.5) for 15 degrees of freedom (ndf), a 4.2σ ($\gg 5\sigma$) confidence level (CL) statistical incompatibility. A comparison between μCAR and πCAR blip samples yields a χ^2/ndf of 40.86/15, indicating 3.6σ incompatibility in these two samples. Thus, we have provided the first observation of the products of stopped pion and muon nuclear capture on argon, and we have shown that nuclear capture products can be used to differentiate muon and pion samples in LArTPC data.

A comparison of blip attributes between data and MC for μCAR or πCAR signals is provided in Table II and Fig. 3. Other blip attributes of interest for data and MC, such as individual blips' E_{blip} and (x, y, z) positions and events' summed blip count and E_{blip}, are pictured in SM [46]. The MeV-scale content present in LArIAT MC events for both muon and pion nuclear captures at rest is substantially larger than that observed in data.

A detailed comparison of data and MC μCAR or πCAR blip samples was performed using a pulls-approach χ^2 test statistic,

$$\chi^2 = \sum_i \left(\frac{\{[S_i^{\text{MC}}(1+\eta_S) - T_i^{\text{MC}}](1+\eta_C) - [S_i^D - T_i^D(1+\eta_B)]\}^2}{\sigma_{\text{stat}}^2} \right) + \frac{\eta_B^2}{\sigma_B^2} + \frac{\eta_S^2}{\sigma_S^2} + \frac{\eta_C^2}{\sigma_C^2}. \quad (1)$$

In this equation, per-event signal (S) and background (T) content are considered in each vertex-blip distance bin i for data (D) and MC. The statistical uncertainty σ_{stat} of each bin considers signal and background contributions for MC and data.

Nuisance parameters η account for the impact of systematic error sources, with pull terms constraining η at a level dictated by the size of the associated uncertainty, σ. Background parameter η_B is treated as a normalization uncertainty with σ_B of 5.5%. Uncertainties in simulated detector response, including electron lifetime, reconstructed energy scales, and blip detection thresholds are accounted for with η_C; a quadrature-summed normalization uncertainty of $\sigma_C = 3.0\%$ was defined by observing changes in blip counts in MC samples with varied detector response parameters. A signal normalization uncertainty η_S

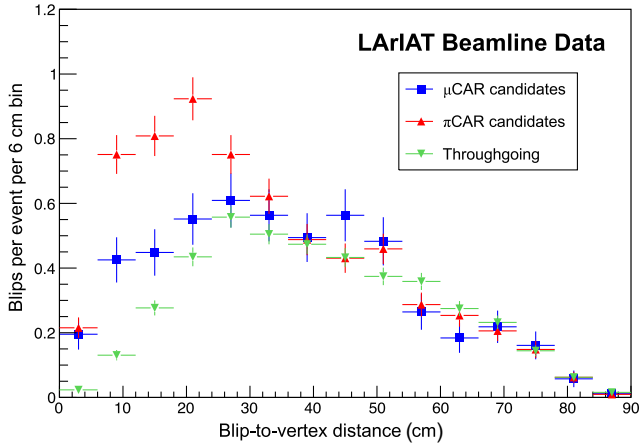

FIG. 2. Distance between reconstructed blips and their associated signal track endpoints for muon (blue squares) and pion (red triangles) nuclear capture-at-rest datasets. This metric is also provided for blips in the throughgoing track dataset, with distances given with respect to a randomly chosen signal track endpoint as described in the text. Error bars represent statistical uncertainties.

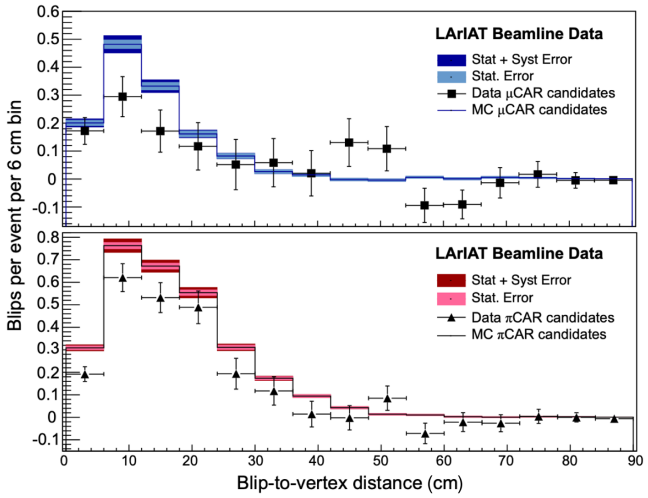

FIG. 3. Distance between reconstructed blips and signal track endpoints for background-subtracted muon (top) and pion (bottom) nuclear capture-at-rest datasets for data (data points) and Monte Carlo (solid lines). For data, vertical (horizontal) bars represent statistical errors (bin widths), while for Monte Carlo, statistical and systematic errors are indicated.

is driven by uncertainties in the beam momentum (p) and track range (L) variables defined above, which are crucial for classifying μCAR and πCAR events. This source is dominated by a 6.4 MeV uncertainty in μ/π energy loss between wire chamber and LArTPC elements, caused primarily by a plastic scintillator halo paddle traversed by a subset of beam particles. A 6.4 MeV energy loss (2.6 cm track length) smearing applied to the μ/π classification increases blip counts by 3.2% for μCAR and decreases counts 1.3% for πCAR. Thus, σ_S is assigned as 3.2% (1.3%) for μCAR (πCAR), with η_S constrained to float only to positive (negative) values. Combining and propagating MC statistical errors and σ_B, σ_S, and σ_C 1σ uncertainty values yields 6.2% (3.9%) fractional error in predicted total blip counts of 1.22 (2.34) for μCAR (πCAR) MC samples.

Calculating the test statistic in Eq. (1) for the data and MC samples, we obtain a χ^2 of 22.07 and 21.32 with 12 degrees of freedom (15 bins with 3 fit parameters) for μCAR and πCAR, respectively. These χ^2 correspond to p values of 0.037 and 0.046 for μCAR and πCAR, indicating statistical incompatibility of the data and MC at 2.1σ and 2.0σ CL.

Based on this χ^2 comparison, it appears that data-MC discrepancies are unlikely to be explained by mismodeling of detector, beam, or blip background attributes. A truth-level selection of only simulated events containing a nuclear capture at rest results in marginal shifts in MC-predicted per-event blip counts (0.1 per event), indicating that non-CAR μ/π interaction processes present in the selected samples play at most a subdominant role in the observed overprediction. To further verify the impact of non-CAR background events, we performed a check of average blip counts for a sample of events depicted in Fig. 1 of SM [46] falling outside the $L > 0.41p - 86.5$ particle range requirement defining the πCAR sample, which is enriched in events containing inelastic scattering and absorption of low-momentum in-flight π. This sideband has average blip counts of 1.57 ± 0.15 and 1.90 ± 0.04 per event for data and MC, respectively; this data-MC bias is too small to account for the $\sim$0.5 blip-per-event offset present in the 75%-pure πCAR sample. We note that this sideband's data-MC bias suggests problematic GEANT4 modeling of the final-state products of energetic π-Ar inelastic collisions, contrasting with recent demonstrations of accurate GEANT4 modeling of π-Ar hadronic scattering rates [44]. Proper GEANT4 simulation of the μCAR sample's primary muon decay at rest background has been demonstrated previously by LArIAT [30] and other LArTPC experiments [49,50].

We thus conclude that GEANT4 modeling of the capture process and subsequent nuclear deexcitation is the likely the cause of the discrepancy. This conclusion is supported by a comparison of the prevalence of different μCAR final-state nuclei in MC to those provided in Ref. [31]. The MC reports 29% (9%) ^{40}Cl (^{39}Cl) in the final state, while Ref. [31] measures 7% (49%), suggesting underprediction of pole-term knockout of the capturing nucleon [51]. Meanwhile, the MC reports 36% of final-state nuclei having $A < 38$, while this population is entirely absent in Ref. [31], indicating incorrect modeling of nuclear evaporation and other deexcitation processes. If μCAR MC results are reweighted according to the measured prevalence of final-state nuclei reported in Ref. [31], the resulting average predicted blip count, 0.9 per event, is statistically consistent with data, and the data-MC χ^2/ndf pictured in Fig. 3 is reduced from 22.07/12 to 11.94/12. This improved agreement clearly illustrates the potential impact inaccurate nuclear modeling can have on predicted MeV-scale activity associated with muon or pion capture in an LArTPC.

In summary, we have used the LArIAT LArTPC to perform first measurements of the final-state products of π^- and μ^- nuclear captures at rest on argon. This represents the first demonstration of the utility of blip information for performing particle-type and charge-sign discrimination for pions and muons in LArTPCs. GEANT4-based MC simulations of μCAR and πCAR in LArIAT cannot accurately reproduce the observed blip activity. Thus, improved modeling of these medium-energy nuclear processes is essential in order to fully realize this new and promising LArTPC particle discrimination capability.

Acknowledgments—This document was prepared by the LArIAT Collaboration using the resources of Fermilab, a U.S. Department of Energy, Office of Science, HEP User Facility. Fermilab is managed by Fermi Research Alliance, LLC (FRA), acting under Contract No. DE-AC02-07CH11359. We extend a special thank you to the coordinators and technicians of the Fermilab Test Beam Facility, without whom this work would not have been possible. This work was directly supported by the National Science Foundation (NSF) through Grant No. PHY-1555090. We also gratefully acknowledge additional support from the NSF; Brazil CNPq Grant No. 233511/2014–8; Coordenação de Aperfeiçoamento de Pessoal de Nível Superior-Brazil (CAPES)-Finance Code 001; São Paulo Research Foundation-FAPESP (BR) Grant No. 16/22738-0; the Science and Technology Facilities Council (STFC), part of the United Kingdom Research and Innovation; The Royal Society (United Kingdom); the Polish National Science Centre Grant No. Dec-2013/09/N/ST2/02793; the JSPS grant-in-aid (Grant No. 25105008), Japan; and the Science and Technology Facilities Council (STFC) Grant No. ST/W003945/1. M. H.-M. was supported by the Visiting Scholars Award Program of the Universities Research Association and the Starr-Fieldhouse Research Fellowship at the Illinois Institute of Technology.

[1] R. Acciarri *et al.* (ArgoNeuT Collaboration), Demonstration of MeV-scale physics in liquid argon time projection chambers using ArgoNeuT, Phys. Rev. D **99**, 012002 (2019).

[2] R. Acciarri *et al.* (ArgoNeuT Collaboration), Improved limits on millicharged particles using the ArgoNeuT experiment at Fermilab, Phys. Rev. Lett. **124**, 131801 (2020).

[3] P. Abratenko (MicroBooNE Collaboration), Observation of radon mitigation in MicroBooNE by a liquid argon filtration system, J. Instrum. **17**, P11022 (2022).

[4] P. Abratenko *et al.* (MicroBooNE Collaboration), Measurement of ambient radon progeny decay rates and energy spectra in liquid argon using the MicroBooNE detector, Phys. Rev. D **109**, 052007 (2024).

[5] W. Castiglioni, W. Foreman, I. Lepetic, B. R. Littlejohn, M. Malaker, and A. Mastbaum, Benefits of MeV-scale reconstruction capabilities in large liquid argon time projection chambers, Phys. Rev. D **102**, 092010 (2020).

[6] B. Abi *et al.* (DUNE Collaboration), Supernova neutrino burst detection with the Deep Underground Neutrino Experiment, Eur. Phys. J. C **81**, 423 (2021).

[7] S. Andringa *et al.*, Low-energy physics in neutrino LArTPCs, J. Phys. G **50**, 033001 (2023).

[8] S. Kubota *et al.* (Q-Pix Collaboration), Enhanced low-energy supernova burst detection in large liquid argon time projection chambers enabled by Q-Pix, Phys. Rev. D **106**, 032011 (2022).

[9] T. Bezerra *et al.*, Large low background kTon-scale liquid argon time projection chambers, J. Phys. G **50**, 060502 (2023).

[10] P. Adamson *et al.* (MINOS Collaboration), Measurement of neutrino and antineutrino oscillations using beam and atmospheric data in MINOS, Phys. Rev. Lett. **110**, 251801 (2013).

[11] M. A. Acero *et al.* (NOvA Collaboration), First measurement of neutrino oscillation parameters using neutrinos and antineutrinos by NOvA, Phys. Rev. Lett. **123**, 151803 (2019).

[12] K. Abe *et al.* (T2K Collaboration), T2K measurements of muon neutrino and antineutrino disappearance using 3.13×10^{21} protons on target, Phys. Rev. D **103**, L011101 (2021).

[13] A. A. Aguilar-Arevalo *et al.* (MiniBooNE Collaboration), Measurement of neutrino-induced charged-current charged pion production cross sections on mineral oil at $E_\nu \sim 1$ GeV, Phys. Rev. D **83**, 052007 (2011).

[14] A. Higuera *et al.* (MINERvA Collaboration), Measurement of coherent production of $\pi^{\pm}$ in neutrino and antineutrino beams on carbon from E_ν of 1.5 to 20 GeV, Phys. Rev. Lett. **113**, 261802 (2014).

[15] R. Acciarri *et al.* (ArgoNeuT Collaboration), First measurement of neutrino and antineutrino coherent charged pion production on argon, Phys. Rev. Lett. **113**, 261801 (2014); **114**, 039901(E) (2015).

[16] K. Abe *et al.* (T2K Collaboration), First measurement of the muon neutrino charged current single pion production cross section on water with the T2K near detector, Phys. Rev. D **95**, 012010 (2017).

[17] K. Abe *et al.* (T2K Collaboration), Measurement of coherent π^+ production in low energy neutrino-carbon scattering, Phys. Rev. Lett. **117**, 192501 (2016).

[18] T. Le *et al.* (MINERvA Collaboration), Measurement of $\bar{\nu}_\mu$ charged-current single π^- production on hydrocarbon in the few-GeV region using MINERvA, Phys. Rev. D **100**, 052008 (2019).

[19] A. Bercellie *et al.* (MINERvA Collaboration), Simultaneous measurement of muon neutrino $\nu\mu$ charged-current single $\pi+$ production in CH, C, H2O, Fe, and Pb targets in MINERvA, Phys. Rev. Lett. **131**, 011801 (2023).

[20] K. Abe *et al.* (T2K Collaboration), Measurements of the $\nu\mu$ and $\nu^-\mu$-induced coherent charged pion production cross sections on C12 by the T2K experiment, Phys. Rev. D **108**, 092009 (2023).

[21] M. Breitbach, L. Buonocore, C. Frugiuele, J. Kopp, and L. Mittnacht, Searching for physics beyond the Standard Model in an off-axis DUNE near detector, J. High Energy Phys. 01 (2022) 048.

[22] A. M. Abdullahi *et al.*, The present and future status of heavy neutral leptons, J. Phys. G **50**, 020501 (2023).

[23] W. Altmannshofer, S. Gori, M. Pospelov, and I. Yavin, Neutrino trident production: A powerful probe of new physics with neutrino beams, Phys. Rev. Lett. **113**, 091801 (2014).

[24] A. de Gouvêa, P. J. Fox, R. Harnik, K. J. Kelly, and Y. Zhang, Dark tridents at off-axis liquid argon neutrino detectors, J. High Energy Phys. 01 (2019) 001.

[25] P. Abratenko *et al.* (MicroBooNE Collaboration), Search for heavy neutral leptons decaying into muon-pion pairs in the MicroBooNE detector, Phys. Rev. D **101**, 052001 (2020).

[26] K. Abe *et al.* (T2K Collaboration), Search for heavy neutrinos with the T2K near detector ND280, Phys. Rev. D **100**, 052006 (2019).

[27] P. Abratenko *et al.* (MicroBooNE Collaboration), Search for long-lived heavy neutral leptons and Higgs portal scalars decaying in the MicroBooNE detector, Phys. Rev. D **106**, 092006 (2022).

[28] D. G. Michael *et al.* (MINOS Collaboration), The magnetized steel and scintillator calorimeters of the MINOS experiment, Nucl. Instrum. Methods Phys. Res., Sect. A **596**, 190 (2008).

[29] K. Abe *et al.*, T2k nd280 upgrade–technical design report, arXiv:1901.03750.

[30] W. Foreman *et al.* (LArIAT Collaboration), Calorimetry for low-energy electrons using charge and light in liquid argon, Phys. Rev. D **101**, 012010 (2020).

[31] A. Klinskikh, S. Brianson, V. Brudanin *et al.*, Muon capture in Ar. The muon lifetime and yields of Cl isotopes., Bull. Russ. Acad. Sci. Phys. **72**, 735 (2008).

[32] S. Agostinelli *et al.*, GEANT4-A simulation toolkit, Nucl. Instrum. Methods Phys. Res., Sect. A **506**, 250 (2003).

[33] T. T. Böhlen, F. Cerutti, M. P. W. Chin, A. Fassò, A. Ferrari, P. G. Ortega, A. Mairani, P. R. Sala, G. Smirnov, and V. Vlachoudis, The FLUKA code: Developments and challenges for high energy and medical applications, Nucl. Data Sheets **120**, 211 (2014).

[34] C. Volpe, N. Auerbach, G. Colo, T. Suzuki, and N. Van Giai, Microscopic theories of neutrino C-12 reactions, Phys. Rev. C **62**, 015501 (2000).

[35] S. Gardiner, Simulating low-energy neutrino interactions with MARLEY, Comput. Phys. Commun. **269**, 108123 (2021).

[36] F. Capozzi, S. W. Li, G. Zhu, and J. F. Beacom, DUNE as the next-generation solar neutrino experiment, Phys. Rev. Lett. **123**, 131803 (2019).
[37] A. Abed Abud *et al.* (DUNE Collaboration), Impact of cross-section uncertainties on supernova neutrino spectral parameter fitting in the Deep Underground Neutrino Experiment, Phys. Rev. D **107**, 112012 (2023).
[38] C. Andreopoulos *et al.*, The GENIE neutrino Monte Carlo generator, Nucl. Instrum. Methods Phys. Res., Sect. A **614**, 87 (2010).
[39] O. Buss, T. Gaitanos, K. Gallmeister, H. van Hees, M. Kaskulov, O. Lalakulich, A. Larionov, T. Leitner, J. Weil, and U. Mosel, Transport-theoretical description of nuclear reactions, Phys. Rep. **512**, 1 (2012), transport-theoretical Description of Nuclear Reactions.
[40] T. Golan, J. Sobczyk, and J. Zmuda, Nuwro: The wroclaw Monte Carlo generator of neutrino interactions, Nucl. Phys. B, Proc. Suppl. **229–232**, 499 (2012).
[41] Y. Hayato and L. Pickering, The NEUT neutrino interaction simulation program library, Eur. Phys. J. Spec. Top. **230**, 4469 (2021).
[42] R. Acciarri *et al.* (LArIAT Collaboration), The liquid argon in a testbeam (LArIAT) experiment, J. Instrum. **15**, P04026 (2020).
[43] B. Baller, Liquid argon TPC signal formation, signal processing, and reconstruction techniques, J. Instrum. **12**, P07010 (2017).
[44] E. Gramellini *et al.* (LArIAT Collaboration), Measurement of the $\pi -$ Ar total hadronic cross section at the LArIAT experiment, Phys. Rev. D **106**, 052009 (2022).
[45] M. Antonello *et al.*, Precise 3D track reconstruction algorithm for the ICARUS T600 liquid argon time projection chamber detector, Adv. High Energy Phys. **2013**, 260820 (2013).
[46] See Supplemental Material at http://link.aps.org/supplemental/10.1103/PhysRevLett.134.131801 for the LArIAT beamline and blip attributes.
[47] T. J. Roberts and D. M. Kaplan, G4BEAMLINE simulation program for matter-dominated beamlines, in *2007 IEEE Particle Accelerator Conference (PAC)* (2007), pp. 3468–3470.
[48] E. Snider and G. Petrillo, LARSOFT: Toolkit for simulation, reconstruction and analysis of liquid argon TPC neutrino detectors, J. Phys. Conf. Ser. **898**, 042057 (2017).
[49] R. Acciarri *et al.* (MicroBooNE Collaboration), Michel electron reconstruction using cosmic-ray data from the MicroBooNE LArTPC, J. Instrum. **12**, P09014 (2017).
[50] S. Amoruso *et al.* (ICARUS Collaboration), Measurement of the μ decay spectrum with the ICARUS liquid argon TPC, Eur. Phys. J. C **33**, 233 (2004).
[51] D. Measday, The nuclear physics of muon capture, Phys. Rep. **354**, 243 (2001).